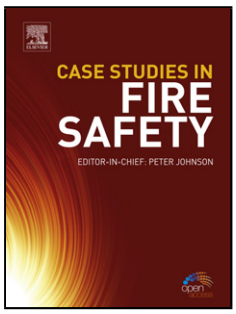

Title: Evaluation of multi-layered graphene nano-platelet composite coatings for corrosion control Part II – Cathodic delamination kinetics

Authors: C.F. Glover, C.A.J. Richards, G. Williams, H.N. McMurray

PII: S0010-938X(17)32115-7
DOI: https://doi.org/10.1016/j.corsci.2018.03.014
Reference: CS 7430

To appear in:

Received date: 24-11-2017
Revised date: 8-3-2018
Accepted date: 10-3-2018

Please cite this article as: Glover CF, Richards CAJ, Williams G, McMurray HN, Evaluation of multi-layered graphene nano-platelet composite coatings for corrosion control Part II – Cathodic delamination kinetics, *Corrosion Science* (2010), https://doi.org/10.1016/j.corsci.2018.03.014

Evaluation of multi-layered graphene nano-platelet composite coatings for corrosion control Part II – Cathodic delamination kinetics

C.F. Glover[b], C.A.J. Richards*[,a], G. Williams[a], H.N. McMurray[a]

[a] *Materials Research Centre, College of Engineering, Swansea University, Bay Campus, Fabian Way, Swansea, UK, SA1 8EN.*

[b] *Centre of Electrochemical Science and Engineering, University of Virginia, McCormick Avenue, Charlottesville, Virginia, USA, VA22904*

*Corresponding author: Tel: 07889271936
E-mail address: 557333@swansea.ac.uk

Highlights

- Graphene nano-platelets (GNP) reduce corrosion-driven cathodic delamination rates.
- GNP act principally to slow through-coating oxygen diffusion when coated on iron.
- When the GNP are coated on zinc, a galvanic couple is formed.
- The galvanic coupling of the GNP and zinc may displace cathodic oxygen reduction.

Abstract

In-situ Scanning Kelvin probe (SKP) measurements are used to follow the corrosion-driven cathodic delamination kinetics of model coatings comprising graphene nano-platelets (GNP) dispersed in polyvinylbutyral (PVB) adherent to iron and zinc (galvanised steel). To reduce delamination rates by >90% (relative to unpigmented PVB) a GNP volume fraction of 0.056 is required on iron but only 0.028 on zinc. On this basis, together with work function and O_2 permeability data it is proposed that the GNP acts principally to slow through-coating oxygen transport on iron; whereas on zinc a galvanic couple forms between zinc and GNP, displacing cathodic oxygen reduction.

Keywords: Graphene nano-platelets, scanning Kelvin probe, cathodic delamination, iron, zinc.

1. Introduction

The benefit of graphene and graphene-composites for corrosion protection is a current topic of interest [1–5] and the principal mechanism by which inhibition occurs is a contentious issue. Many publications speculate that reduced permeation to oxygen and water is the principal mechanism, (Fig. 1.b)[4,6–15].Others suggest that the electrical conductivity of graphene enables it to support electron transfer reactions, displacing electrochemical activity away from the metal surface and into the graphene coating (Fig. 1.c)[2,5,16]. These mechanisms are illustrated schematically in Fig. 1. Thus, in Fig. 1a an unpigmented, electronically non-conductive coating allows relatively facile O_2 transport and cathodic O_2 reduction occurs at the metal-coating interface. In Fig. 1b a GNP-polymer composite coating exhibits reduced O_2 permeability due to the increased tortuosity of O_2 diffusion pathways. In Fig.1c electronic conduction pathways from the metal substrate through and interconnected network of GNP particles allows cathodic O_2 reduction to become displaced from the metal coating interface and into the coating. Conversely, it should be noted that making the coating a cathode might have a corrosion accelerating effect where metal is exposed at a coating defect due to coating-defect coupling. Here, we aim to establish the dominant mechanism for hot dip galvanised steel (HDG) and iron substrates using the Scanning Kelvin probe technique (SKP), and findings from Part I of this paper, to assess the effect of in-coating GNP on an important failure mechanism, cathodic delamination.

Figure 1

In the case of unpigmented polymer coatings, delamination is driven by an electrochemical cell via the galvanic coupling of anodic metal dissolution in the defect region with cathodic oxygen reduction at the advancing delamination front (Eq. 1 and Eq. 2 respectively) as depicted in the schematic in Fig.2. The electrochemical reduction of molecular O_2 leads to the generation of OH^- ions that render the cathodic delamination zone highly alkaline (i.e. > pH 10)[17,18].

Figure 2

The formation of hydroxyl radicals as intermediates in the cathodic reduction of oxygen has also been implicated in attacking the organic binder by oxidative degradation [17]. A thin, gel-like layer of electrolyte ingresses underneath the coating and loss of adhesion is widely attributed to alkaline attack on the coating-metal bond [19](Eq. 4).

$$M \rightleftharpoons M^{n+} + ne^- \qquad \text{eq. [1]}$$

$$O_2 + 2\,H_2O + 4e^- \rightleftharpoons 4OH^- \qquad \text{eq. [2]}$$

In the current study, experiments were carried out on iron and HDG substrates in high humidity (95%) air where a 0.86 M aqueous NaCl electrolyte was added to a penetrating defect. By systematically varying the non-functionalised graphene nano-platelet (GNP) content dispersed in polyvinyl butyral (PVB) primer coatings in contact with the substrate, it was possible to assess the rate and time dependent order of cathodic delamination kinetics. The SKP technique is a well-established method for determining the kinetics of corrosion-driven organic coating failure/delamination, as a means of establishing the relative efficiency and inhibitive mechanisms of coating containing dispersed inhibitive pigments [20–24] and for various other corrosion studies [25–27]. The oxygen permeation, conductivity and Volta potential data presented in Part I of this paper have been used to support our hypotheses.

2. Materials and methods

Materials: Iron foil (99.99% purity) of 1.5 mm thickness was obtained from Goodfellow Metals Ltd. This was cut into square coupons of 50 mm × 50 mm. Hot dip galvanized steel (HDG) samples, provided by Tata Steel UK, comprising 0.7 mm gauge mild steel coated with a Zn layer of 20 μm (also containing 0.2% Al) were also cut into square coupons of 50 mm × 50 mm. All chemicals were supplied by Sigma-Aldrich Chemical Co and were of analytical grade purity. GNP pigment obtained from Haydale ltd and characterized previously [34] was dispersed in PVB at various pigment volume fractions (ϕ) [34].

Methods: Design and operation of the SKP apparatus has been described extensively elsewhere [20,29,30]. The sample preparation procedure was based on the methods presented in work carried out by Stratmann et al [19,29,33]. Polyvinyl butyral (PVB) solutions MW 70,000-100,000 were prepared in ethanol (15.5% w/w) and the required amount of GNP were added and thoroughly mixed. An aqueous slurry of 5 μm alumina was used to hand-polish the sample surface to remove any contaminants and a pre-existing oxide layer. Degreasing was carried out via an acetone rinse followed by air-drying. PVB solution containing the appropriate amount of GNP was bar-cast onto a pre-cleaned sample and room-air dried. Strong film adhesion was observed in both wet and dry form where it was not possible for the film to be peeled off by hand.

All delamination experiments were carried out in an enclosed SKP chamber maintained at a constant 95% RH and 25˚C. Delamination was initiated on each occasion by introducing ~2 cm^3 of 0.86 M wt/v aqueous NaCl (pH 7) into the penetrative coating defect region. The SKP reference probe consisted of a gold wire of diameter 125 μm vibrating vertically at 280 Hz and amplitude of 40 μm at a distance of 100 μm above the sample surface. $\Delta\Psi_{gold}^{sample}$ data points were recorded at 20 per mm. The SKP reference probe was scanned over the coated surface along a 12 mm line normal to, and adjacent with, the defect-coating boundary. Scanning

commenced immediately on the addition of electrolyte and thereafter at hourly intervals over a period of ≥ 24 h.

3. Results

SKP Potentiometry

When iron or HDG zinc substrates coated with PVB or PVB-GNP were subject to SKP scanning in air at 95% RH the measured values of $\Delta\Psi^{sample}_{gold}$ were found to be substantially uniform over the sample surface and became stable (time-independent) after approximately 2 hours. Fig. 3 shows area-averaged (20 data points per millimetre over a length of 12 mm repeated 4 times and 1 mm apart) time-independent $\Delta\Psi^{sample}_{gold}$ values plotted versus ϕ_{GNP} and it may be seen that for both iron and zinc substrates $\Delta\Psi^{sample}_{gold}$ increases monotonically with ϕ_{GNP}. The significance of $\Delta\Psi^{sample}_{gold}$ for polymer-coated metal has been discussed at length elsewhere [28,31,33]. Briefly, for nonconducting polymers $\Delta\Psi^{sample}_{gold}$ reflects the open-circuit potential of the oxide-covered metal surface, influenced as this may be by reaction with atmospheric O_2 and/or Bronsted acid-base interactions occurring between the oxide and polymer coating. However, as shown in Part I of this paper[34], electronic conductors such as GNP can establish a contact potential when brought into electrical contact with a conducting (metallic) substrate. The results shown in Fig. 3 may therefore be understood in terms of $\Delta\Psi^{sample}_{gold}$ being determined by the redox state of iron surface oxide and non-faradaic oxide-PVB interactions when ϕ_{GNP} = zero, but becoming progressively influenced by the substrate-GNP contact potential as ϕ_{GNP} increases.

Figure 3

For zinc, it may be seen that $\Delta\Psi^{sample}_{gold}$ increases monotonically with ϕ_{GNP} from -0.7 V for ϕ_{GNP} = zero (pure PVB) to 0.24 V for ϕ_{GNP} = 0.056. Further increase in ϕ_{GNP} (up to ϕ_{GNP} - 0.12) produces little additional change in $\Delta\Psi^{sample}_{gold}$ (~ 0.07 V). These findings suggest that any promotion of $\Delta\Psi^{sample}_{gold}$ owing to the development of a GNP-zinc contact potential is substantially complete for $\phi_{GNP} \geq 0.06$. In part I, the value for $\Delta\Psi^{sample}_{gold}$ was found to be ~ 0 V for dry GNP powder in electrical contact with zinc, but a comparison with Fig. 3 shows that, when a PVB-GNP composite coating of $\phi_{GNP} \geq 0.06$ is present, the $\Delta\Psi^{sample}_{gold}$ value was found to be ~ 0.3 V. This apparent discrepancy is explicable on the basis of changes in the surface-air dipole due to the presence of PVB and adsorbed water at 95% RH. Previous work has shown that surface-air dipole potentials can differ by ~ 0.3 V between a water-air and water-PVB air interface [26]. A similar reasoning may be applied in the case of iron, where (Fig. 3) shows that $\Delta\Psi^{sample}_{gold}$ increases by ~ 0.3 V as ϕ_{GNP} is increased from zero to 0.12. The smaller dependency of $\Delta\Psi^{sample}_{gold}$ on ϕ_{GNP} for the iron substrate reflects the smaller iron-GNP contact potential reported in part I of this paper [34].

Final evidence that the ϕ_{GNP} dependent increase in $\Delta\Psi^{sample}_{gold}$ seen in Fig. 3 arises primarily as a result of the GNP-substrate contact potential and not (for example) simply as a result of a ϕ_{GNP} dependent variation in surface dipole was obtained from the experiment shown schematically in Fig. 4. A zinc (HDG) substrate was partially coated with a 16 μm thick layer of unpigmented PVB and then overcoated with smaller area of 16 μm thick PVB-GNP composite (ϕ_{GNP} = 0.056). By so doing the PVB-GNP composite coating was produced in such a way as to be adherent to, but electronically isolated from, the zinc substrate. The SKP then scanned over a length of 8 mm, travelling from a region of the uncoated zinc substrate to the PVB coated substrate and finally the PVB-GNP overcoated PVB coated substrate. Scans were

taken at 1 hour intervals for a 12-hour period in air at 95%RH and became stable (repeatable) after 2 hours. The time-independent Volta potential profile thus obtained is shown superimposed on the experimental geometry in Fig. 4. It may be seen that no significant change in $\Delta\Psi_{gold}^{sample}$ was observed between the PVB coated and PVB-GNP over-coated regions of the sample. The increase in $\Delta\Psi_{gold}^{sample}$ of approximately 320 mV which occurs when scanning from the bare zinc (HDG) surface to the PVB coated surface may reasonably be attributed to the polymer-air dipole contribution. A change in potential of approximately 220 mV was previously reported when air-water was replaced with an air-PVB. [31]. These findings tend to confirm that the large increase in $\Delta\Psi_{gold}^{sample}$ observed with increasing ϕ_{GNP} (Fig. 3) must result primarily from a GNP-substrate contact potential. It should be noted $\Delta\Psi_{gold}^{sample}$ over the bare zinc (HDG) surface is approximately -1100mV which is slightly less negative than the value of -1200mV reported for pure zinc in Part I of this paper. This difference reflects the relative impurity of the HDG zinc layer and the difference of RH (95% here *vs* 50% in Part I [34]).

Figure 4

Delamination of PVB coatings on iron

For unpigmented PVB adherent to an iron substrate, corrosion-driven cathodic delamination became initiated within 2 hours of electrolyte introduction at the coating defect and was identified by the development of distinctive time-dependent $\Delta\Psi_{gold}^{sample}$ *vs.* distance profiles, as shown in Fig. 5a. These profiles are produced by ionic current flux passing along the thin layer of electrolyte which ingresses beneath the delaminated coating and producing an ohmic potential gradient linking the anodic site at the coating defect (Eq. 1) to the site of cathodic oxygen reduction (Eq. 2) at the coating delamination front [24]. Fig. 5b shows representative $\Delta\Psi_{gold}^{sample}$ *vs.* distance profiles for a PVB-GNP composite coating containing a

GNP volume fraction (ϕ_{GNP}) of 0.056. A comparison of Figs. 5a and 5b shows that the extent of delamination produced after a holding period of 24 h becomes significantly reduced (relative to unpigmented PVB) when GNP pigment is present.

Figure 5

It should be noted that in previous publications where SKP has been used to follow the kinetics of cathodic disbondment, $\Delta\Psi$ values have typically been converted to values of electrochemical potential or free corrosion potential. The calibration method for so doing is straightforward and has been described in detail elsewhere. However, because of the evolution of metal-GNP contact potentials, described in part 1 of this paper, we believe that a conversion to electrochemical potential might be inappropriate and misleading in the case of GNP pigmented coatings. For this reason, all subsequent results will be presented and discussed in terms of unconverted $\Delta\Psi$ values.

Values of $\Delta\Psi_{gold}^{sample}$ measured in the intact (undelaminated) coated region remained stable throughout the experiment and were entirely similar to those reported in Fig. 3. The position of the delamination front is taken as the midpoint of the sharp drop in potential from the intact coating region, as described previously [19]. Delamination kinetics were determined by plotting delaminated distance (x_{del}) against time minus the time for delamination to become initiated (t_{del} - t_i) as shown in Fig.6. A marked change was observed in delamination kinetics when GNP pigments were introduced into the coating. Systematically increasing ϕ_{GNP} was found to produce a progressive reduction in delamination rate but also a change in kinetic order with respect to time, from parabolic ($t^{1/2}$ dependence) to zero order (linear with respect to t). These effects are clearly shown in the curves plotted in Fig. 6, where only the curve derived from unpigmented PVB plot shows deviation from linearity.

Figure 6

Delamination of PVB-GNP coatings from HDG substrates

When delamination experiments were carried out using unpigmented PVB coatings adherent to zinc (HDG) substrates, the initiation time for delamination was found to be similar to that for iron surfaces, i.e. within 2 h of electrolyte being added to the penetrating defect. Thereafter, time-dependent $\Delta\Psi_{gold}^{sample}$ vs. distance profiles became established as shown in Fig. 7a. Fig. 7b shows representative $\Delta\Psi_{gold}^{sample}$ vs. distance profiles obtained from a PVB-GNP composite coating containing a GNP volume fraction (ϕ_{GNP}) of 0.028. A comparison of Figs. 7a and 7b shows that the extent of delamination produced after a holding period of 24 h becomes significantly reduced (relative to unpigmented PVB) when GNP pigment is present. Again, values of $\Delta\Psi_{gold}^{sample}$ measured in the intact (undelaminated) coated region remained stable throughout the experiment and were entirely similar to those reported in Fig. 3. As in the case or iron, systematically increasing ϕ_{GNP} was found to produce a progressive reduction in delamination rate but, in contrast to iron, no change in kinetic order was observed – ie. delamination kinetics remained parabolic. Plots of x_{del} vs. $(t_{del} - t_i)^{1/2}$, are shown for various ϕ_{GNP} in Fig. 8 and it may be seen that all the curves retain linearity for both unpigmented and pigmented PVB coatings.

Figure 8

3. Discussion

For uninhibited PVB coatings, it has been demonstrated previously that delamination from iron and HDG surfaces is controlled by the under-film mass transport (migration) of cations (in this case Na^+) from the defect site to the cathodic delamination front [29], giving rise to parabolic delamination kinetics (half order with respect to time) in which x_{del} increases as $(t-t_i)^{1/2}$.

This behaviour is clearly the case for unpigmented PVB coatings on both iron (Fig. 6, curve i) and zinc (Fig. 8, curve i). However, as the volume fraction of GNP in the PVB-GNP coatings is increased, a marked deviation in behaviour is observed between the iron and zinc substrates. In the case of zinc (Fig. 8, curves ii - v) the x_{del} vs. $(t-t_i)^{1/2}$ plots remain linear throughout. In the case of iron (Fig. 6, curves ii - v), the kinetics become substantially linear (zero order with respect to time) for all GNP $\geq$ 0.028.

The first implication of the above findings is that, for the zinc substrate, coating delamination rates remain controlled by the under-film Na^+ cation migration, albeit with a parabolic rate constant (k_{del}) which decreases with increasing ϕ_{GNP}. Results of this nature could be produced by either: i) GNP pigmentation acting to increase the tortuosity or difficulty of the Na^+ migration pathway or ii) GNP pigmentation acting to increase the quantity of charge required (and therefore the number of Na^+ ions) to pass through the delamination cell to produce unit delamination. The second implication is that, for the iron substrate, Na^+ migration ceases to be rate controlling for all $\phi_{GNP} \geq 0.028$. A result of this nature is consistent with a vertical process (one not dependent on x_{del}) becoming rate determining as ϕ_{GNP} increases, such a vertical process could be either: i) diffusional mass transport of O_2 through the coating or ii) the electrochemical electron transfer process associated with the cathodic oxygen reduction reaction (Eq. 2).

In assessment of the above, we can eliminate the theories that do not hold up for both substrates. Any increase in the tortuosity of under-film Na^+ migration pathways produced directly by the presence of GNP particles in the PVB-GNP coating would be expected to be identical for iron and zinc surfaces. As the effects of increasing ϕ_{GNP} on delamination kinetics are very different for iron and zinc (Figs. 6 and 8), this hypothesis is unlikely and can be eliminated. Likewise, any reduction in cathodic electron transfer rate caused by the PVB-GNP

coating on iron substrates would also be expected to occur on the zinc surface. The failure to observe linear (zero order) delamination kinetics for zinc surfaces in the presence of GNP additions again renders this hypothesis unlikely.

The linear delamination kinetics demonstrated for iron surfaces when GNP pigment is present (Fig. 6) are immediately consistent with the notion of vertical O_2 mass transport becoming rate determining due to an increase in the tortuosity of O_2 diffusion pathways, as shown schematically in Fig. 1c. It can also be shown that the delamination rates correlate well with the through-coating O_2 permeation data previously measured for the PVB-GNP coating [34]. Fig. 9, curve (iii) shows dimensionless delamination rates obtained from the various x_{del} vs. $(t_{del}-t_i)$ slopes in Fig. 6 plotted versus ϕ_{GNP}. The delamination rates are all normalised to the initial rate in the case of $\phi_{GNP} = 0$ (where it is assumed that, as x_{del} and cation migration length tends to zero, under-film cation migration ceases to be rate limiting). Curve (ii) in Fig. 9 shows the corresponding through-coating O_2 permeabilities, again dimensionless and normalized to the permeability for $\phi_{GNP} = 0$ (pure PVB). It may be seen that curves (iii) and (ii) of Fig. 9 are very similar and fractional reductions in coating delamination rate are of the same magnitude as the fractional reduction in O_2 permeability.

Figure 9

For zinc, cathodic delamination kinetics are significantly more sensitive to GNP additions than is the case for iron. Curve (i) in Fig. 9 shows dimensionless parabolic delamination rate constants obtained from the various x_{del} vs. $(t_{del}-t_i)^{1/2}$ slopes in Fig. 8 plotted versus ϕ_{GNP}. The rate constants are all normalised to the rate constant in the case of $\phi_{GNP} = 0$ (pure PVB). In contrast to iron, a comparison made between curves (i) and (iii) of Fig. 9 shows a very poor correlation between delamination rate constant and through-coating O_2 permeability. The measured fractional reductions in delamination rate constant are many times

(4.5) the fractional reduction in O_2 permeability at intermediate values (0.028) of $\phi_{GNP.}$ These findings, taken together with the retention of parabolic delamination kinetics on zinc could be explained on the basis of an increase in the amount of charge (the number of Na^+ ions) required to produce unit delamination on zinc. This, in turn, could be explained on the basis of a displacement of the cathodic reduction reaction away from the metal substrate coating interface and into the coating, as shown schematically in Fig. 1c.

Metal-GNP contact potential difference of ~0.6 V and ~1.2 V were measured for iron and zinc respectively [34]. Furthermore, the relative magnitude of these contact potentials are reflected in variation of coated sample potential difference with increasing ϕ_{GNP} seen in Fig. 3. It has been argued theoretically that the absolute electrode potential of an electronic conductor depends linearly on the work function [35]. Furthermore, it has been demonstrated experimentally that the standard electrode potentials of pure metals correlate well with contact potentials measured using a Kelvin probe [36]. On this basis, the metal-GNP contact potential difference of 0.6 V and 1.2 V measured for iron and zinc, respectively, would be expected to result in metal-GNP galvanic couples with similar galvanic cell potentials under standard conditions. Under the particular conditions of our cathodic disbondment experiments cell potentials may be estimated from the difference between the near-defect $\Delta\Psi_{gold}^{sample}$ values in Figs 5a and 7a (-0.76 V for iron and -1.15 V for zinc) and the $\Delta\Psi_{gold}^{sample}$ values at high Φ_{GNP} in Fig 3. (0.1 V on iron and 0.3 V on zinc). This gives a corroding metal-intact GNP cell potential of approx. -0.86 V in the case of iron and -1.45 V in the case of zinc. Thus on zinc the driving force for making the GNP pigment an oxygen cathode is relatively large and displacement of cathodic activity into the coating is likely, albeit over a short range due to the low electrical conductivity of the PVB-GNP composite (1.48×10^{-5} S m^{-1}) [34]. Conversely, in the case of

iron the driving force is smaller and the GNP pigment is more likely to act simply as an electrochemically inert filler.

If the GNP pigment does, as seems likely, act as an effective oxygen cathode on zinc then the result would be to actually increase corrosion rates, even if the displacement of oxygen reduction (and production of aggressive OH^- ions and free radical oxygen species) away from the coating-metal interface reduces the measured rate of coating delamination. Under these circumstance, the anodic dissolution of zinc which occurs in the alkaline environment existing beneath the delaminated coating [17,37,38] is likely to be accelerated with a consequent increase in the formation and gelatinous, partially hydrolysed zincate solutions. Na^+ mobility in the thin electrolyte layer that forms beneath the delaminating coating is therefore likely to be low (compared to the case on iron, which is passive under alkaline conditions). Thus, in addition to increasing the quantity of cathodic charge (and hence the number of migrated Na^+ cations) required to produce unit area of coating delamination on zinc, the presence of GNP pigment could act indirectly to reduce underfilm Na^+ mobility and so further reduce the value of the parabolic rate constant (k_{del}) for cathodic disbondment on zinc.

4. Conclusions

Graphene Nanoplatelets (GNP) are shown to reduce the measured rate of corrosion-driven organic coating cathodic delamination on both iron and zinc (hot dip galvanised steel) surfaces by up to 93.5% and 99.6% respectively. From the collective findings, presented in Part I and Part II of this paper, we conclude that the principle inhibiting mechanism for cathodic disbondment imparted by GNP differs for the two substrates of interest where:

1. For iron surfaces, vertical diffusion of oxygen through the coating appears to be the rate-limiting process. This is demonstrated by a change from parabolic to linear delamination rate kinetics where the presence of GNP in the coating increases the

tortuosity of molecular pathways for oxygen diffusion. Oxygen permeation data supports this theory and a direct correlation is demonstrated between corrosion-driven delamination rate and the diffusion of oxygen through the coating.

2. For zinc (hot dip galvanised steel, HDG) substrates, the principal role of the GNP is to increased quantity of cathodic charge (and therefore number of migrated Na^+ cations) required to produce unit area of coating delamination. The large contact potential (~1.2 V) measured between the zinc surface and GNP particles represents a significant thermodynamic driving force for the displacement of the cathodic reaction onto GNP. Delamination rates are found to be inhibited to a greater extent at lower pigment volume fractions (ϕ) when compared with the same coatings applied to iron substrates even through the delamination kinetics remain parabolic (limited by underfilm Na^+ migration).

Whatever the exact nature of the influence on cathodic disbondment, the contact potential difference which exists between zinc (and to a less extent iron) and the in-coating GNP pigment is predicted to create a second oxygen reduction site which can compete with and augment the cathodic reaction at the coating-metal interface. As such, this process would be expected to actually increase the rate of metal dissolution at anodic sites despite the observed reduction in cathodic delamination rates. Furthermore, although the GNP pigment additions can slow rates of cathodic delamination on both iron and zinc they do not do so to a technologically useful extent. Taken together, these findings suggest that (although scientifically interesting) the O_2 diffusion blocking and galvanic effects produced by GNP coating pigmentation are not such as to make GNP useful in corrosion protection when used alone.

5. Acknowledgements

The authors recognise the EPSRC, Welsh Government and Tata Steel UK for financial support of this work and Innovate UK for the SPECIFIC Innovation and Knowledge Centre (grant numbers EP/I019278/1, EP/K000292/1, EP/L010372/1). The authors would also like to thank Haydale Ltd for providing materials.

The raw/processed data required to reproduce these findings cannot be shared at this time due to technical or time limitations.

6. References

[1] N.T. Kirkland, T. Schiller, N. Medhekar, N. Birbilis, Exploring graphene as a corrosion protection barrier, Corros. Sci. 56 (2012) 1–4.

[2] S. Böhm, Graphene against corrosion., Nat. Nanotechnol. 9 (2014) 741–2.

[3] B.R. V Dennis, L.T. Viyannalage, V. Anil, Nanocomposite Coatings for Protecting Low- Alloy Steels From Corrosion, Am. Ceram. Soc. Bull. 92 (2013) 18–24.

[4] D. Prasai, J.C. Tuberquia, R.R. Harl, G.K. Jennings, B.R. Rogers, K.I. Bolotin, Graphene: corrosion-inhibiting coating., ACS Nano. 6 (2012) 1102–8.

[5] K. Aneja, S. Bohm, A. Khanna, H. Bohm, Graphene based anticorrosive coatings for Cr(VI) replacement, Nanoscale. 7 (2015) 17879–17888.

[6] C.F. Glover, C. Richards, J. Baker, G. Williams, H.N. McMurray, In-coating graphene nano-platelets for environmentally-friendly corrosion protection of iron, Corros. Sci. 114 (2016) 169–172.

[7] B. Wang, B. V. Cunning, S.Y. Park, M. Huang, J.Y. Kim, R.S. Ruoff, Graphene Coatings as Barrier Layers to Prevent the Water-Induced Corrosion of Silicate Glass, ACS Nano. 10 (2016) 9794–9800.

[8] M. Schriver, W. Regan, W.J. Gannett, A.M. Zaniewski, M.F. Crommie, A. Zettl, Graphene as a long-term metal oxidation barrier: Worse than nothing, ACS Nano. 7 (2013) 5763–5768.

[9] V. Berry, Impermeability of graphene and its applications, Carbon N. Y. 62 (2013) 1–10.

[10] M. Yi, Z. Shen, X. Zhao, L. Liu, S. Liang, X. Zhang, Exploring few-layer graphene and graphene oxide as fillers to enhance the oxygen-atom corrosion resistance of composites., Phys. Chem. Chem. Phys. 16 (2014) 11162–7.

[11] K.C. Chang, M.H. Hsu, H.I. Lu, M.C. Lai, P.J. Liu, C.H. Hsu, et al., Room-temperature cured hydrophobic epoxy/graphene composites as corrosion inhibitor for cold-rolled steel, Carbon N. Y. 66 (2014) 144–153.

[12] Y. Cui, S.I. Kundalwal, S. Kumar, Gas barrier performance of graphene/polymer nanocomposites, Carbon N. Y. 98 (2016) 313–333.

[13] D. Pierleoni, Z.Y. Xia, M. Christian, S. Ligi, M. Minelli, V. Morandi, et al., Graphene-based coatings on polymer films for gas barrier applications, Carbon N. Y. 96 (2016) 503–512.

[14] H. Kim, Y. Miura, C.W. Macosko, Graphene/Polyurethane Nanocomposites for Improved Gas Barrier and Electrical Conductivity, Chem. Mater. 22 (2010) 3441–3450.

[15] O.C. Compton, S. Kim, C. Pierre, J.M. Torkelson, S.T. Nguyen, Crumpled graphene nanosheets as highly effective barrier property enhancers., Adv. Mater. 22 (2010) 4759–63.

[16] K.R. Ratinac, W. Yang, J.J. Gooding, P. Thordarson, F. Braet, Graphene and related materials in electrochemical sensing, Electroanalysis. 23 (2011) 803–826.

[17] G. Grundmeier, W. Schmidt, M. Stratmann, Corrosion protection by organic coatings :

electrochemical mechanism and novel methods of investigation, Electrochim. Acta. 45 (2000) 2515–2533.

[18] H.N. McMurray, G. Williams, Shreir's Corrosion, Elsevier, 2009.

[19] A. Leng, H. Streckel, K. Hofmann, M. Stratmann, The delamination of polymeric coatings from steel Part 3: Effect of the oxygen partial pressure on the delamination reaction and current distribution at the metal/polymer interface, Corros. Sci. 41 (1998) 599–620.

[20] W. Furbeth, M. Stratmann, The delamination of polymeric coatings from electrogalvanized steel - a mechanistic approach. Part 2: delamination from a defect down to steel, Corros. Sci. 43 (2001) 229–241.

[21] G. Williams, H.N. McMurray, M.J. Loveridge, Inhibition of corrosion-driven organic coating disbondment on galvanised steel by smart release group II and Zn(II)-exchanged bentonite pigments, Electrochim. Acta. 55 (2010) 1740–1748.

[22] H.N. McMurray, D. Williams, G. Williams, D.A. Worsley, Inhibitor pretreatment synergies demonstrated using a scanning Kelvin probe technique, Corros. Eng. Sci. Technol. 38 (2003) 112–118.

[23] W. Furbeth, M. Stratmann, The delamination of polymeric coatings from electrogalvanised steel - a mechanistic approach. Part 1: delamination from a defect with intact zinc layer, Corros. Sci. 43 (2001) 207–227.

[24] G. Klimow, N. Fink, G. Grundmeier, Electrochemical studies of the inhibition of the cathodic delamination of organically coated galvanised steel by thin conversion films, Electrochim. Acta. 53 (2007) 1290–1299.

[25] M. Rohwerder, L.M. Duc, a. Michalik, In situ investigation of corrosion localised at the buried interface between metal and conducting polymer based composite coatings, Electrochim. Acta. 54 (2009) 6075–6081.

[26] M. Rohwerder, S. Isik-Uppenkamp, M. Stratmann, Application of SKP for in situ monitoring of ion mobility along insulator/insulator interfaces, Electrochim. Acta. 54 (2009) 6058–6062.

[27] C.F. Glover, J. McGettrick, G. Williams, T.M. Watson, D. Bryant, A Scanning Kelvin Probe Investigation of the Interaction of PEDOT:PSS Films with Metal Surfaces and Potential Corrosion Protection Properties, J. Electrochem. Soc. 162 (2015) H799–H805.

[28] H. Dominighaus, in Plastics for Engineers, p. 142, Hanser Publications, Munich 1988.

[29] W. Fürbeth, M. Stratmann, Scanning Kelvin probe investigations on the delamination of polymeric coatings from metallic surfaces, Prog. Org. Coatings. 39 (2000) 23–29.

[30] M. Stratmann, A. Leng, W. Fürbeth, H. Streckel, H. Gehmecker, K.-H. Groβe-Brinkhaus, The scanning Kelvin probe; a new technique for the in situ analysis of the delamination of organic coatings, Prog. Org. Coatings. 27 (1996) 261–267.

[31] G. Williams and H. N. McMurray, Chromate Inhibition of Corrosion-Driven Organic Coating Delamination Studied Using a Scanning Kelvin Probe Technique J. Electrochem. Soc., 148, B337 2001

[32] R. J. Holness, G. Williams, D. A. Worsley, and H. N. McMurray, Polyaniline Inhibition of Corrosion-Driven Organic Coating Cathodic Delamination on Iron J. Electrochem. Soc., 152, B73 2005.

[33] A. Leng, H. Streckel, and M. Stratmann, The delamination of polymeric coatings from

steel. Part 1: Calibration of the Kelvinprobe and basic delamination mechanism, Corros. Sci., 41, 547 1999.

[34] C. A. Richards, C. F. Glover, H. N. McMurray, G. Williams, J. Baker, Evaluation of Multi-layered Graphene Nano-platelet Composite Coatings for Corrosion Control. Part I Contact Potentials and Gas Permeability. *Submitted for review.*

[35] S. Trasatti, The Absolute Electrode Potential an Explanatory Note, Pure and Applied Chem., 56 (1986) 955-966.

[36] R. Takei, H. H. Imai, J. Umeda and K. Kondoh, Relationship Between Surface Potential Difference and Galvanic Corrosion of Magnesium Alloy Using SKPFM, Transactions of JWRI, 31 (2010) 75-80.

[37] A. Leng, H. Streckel, K. Hofmann, and M. Stratmann, Corros. Sci., The delamination of polymeric coatings from steel Part 3: Effect of the oxygen partial pressure on the delamination reaction and current distribution at the metal/polymer interface (1999) 41, 599

[38] W. Furbeth and M. Stratmann, Corros. Sci., The delamination of polymeric coatings from electrogalvanised steel – a mechanistic approach.: Part 1: delamination from a defect with intact zinc layer (2001) 43, 207.

7. List of Figures

Fig. 1 Schematic showing three scenarios of cathodic delamination where: a) For uninhibited coatings, cathodic O_2 reduction occurs at the coating/substrate interface b) in-coating GNP pigments may d isplace O_2 reduction away from coating/substrate interface c) in-coating GNP pigment may increase the tortuosity of O_2 diffusion pathway.

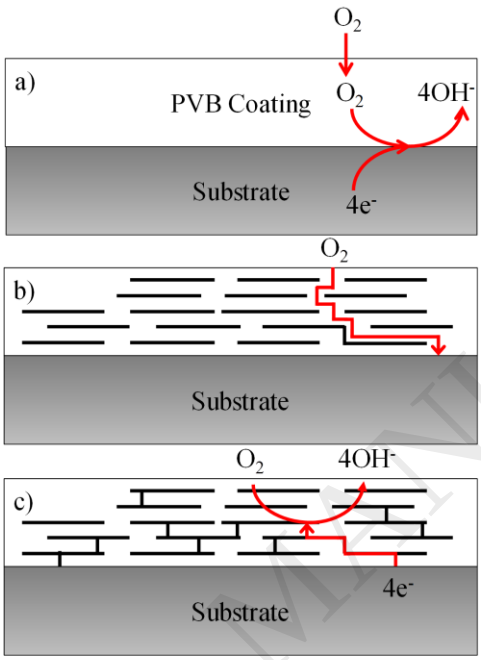

Fig. 2 Schematic representation of the corrosion-driven delamination cell showing correspondence with various regions of the time-dependent $\Delta\Psi_{gold}^{sample}$ profile.

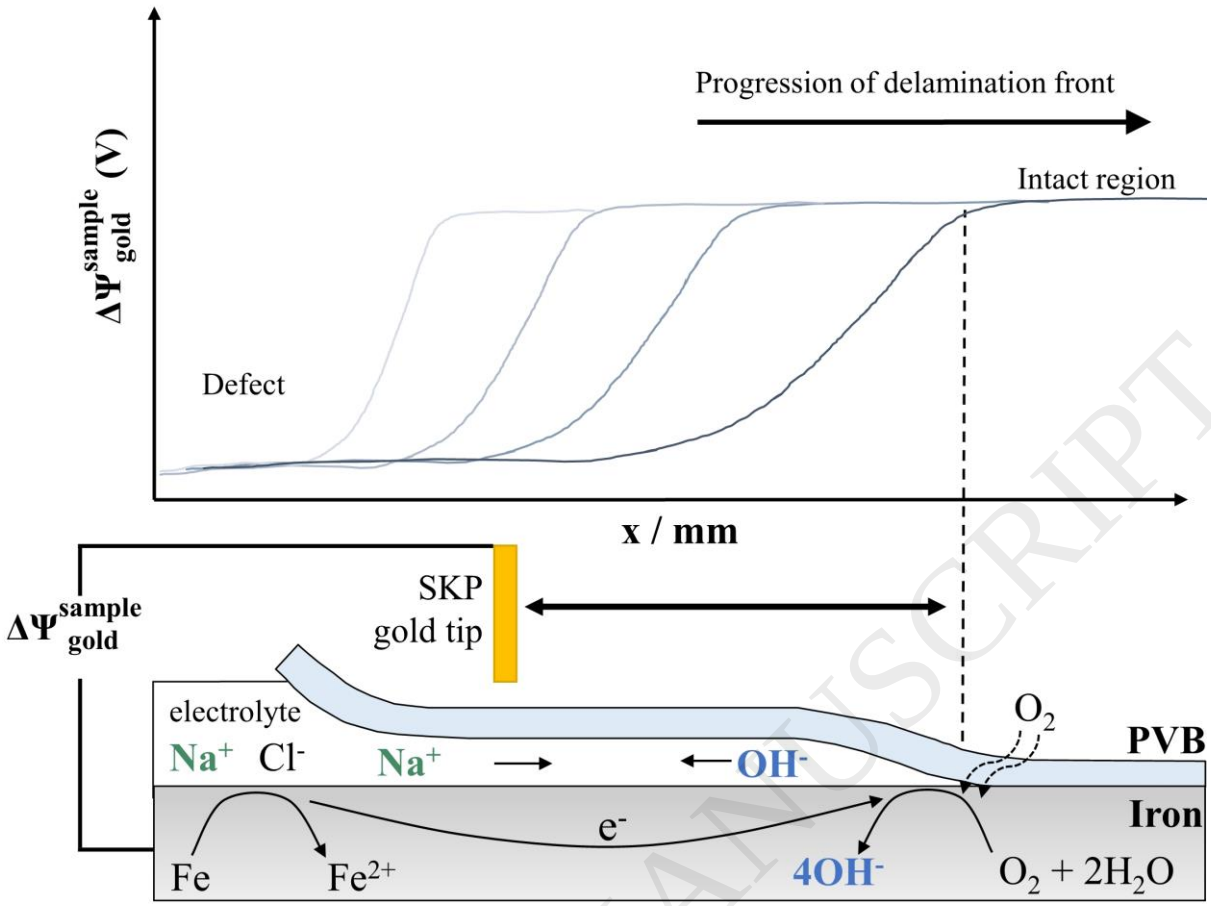

Fig. 3 A plot of the average time independent $\Delta\Psi^{sample}_{gold}$ values measured for the intact region for each of the PVB and PVB-GNP coated samples against respective ϕ_{GNP} for both iron and zinc (HDG) substrates.

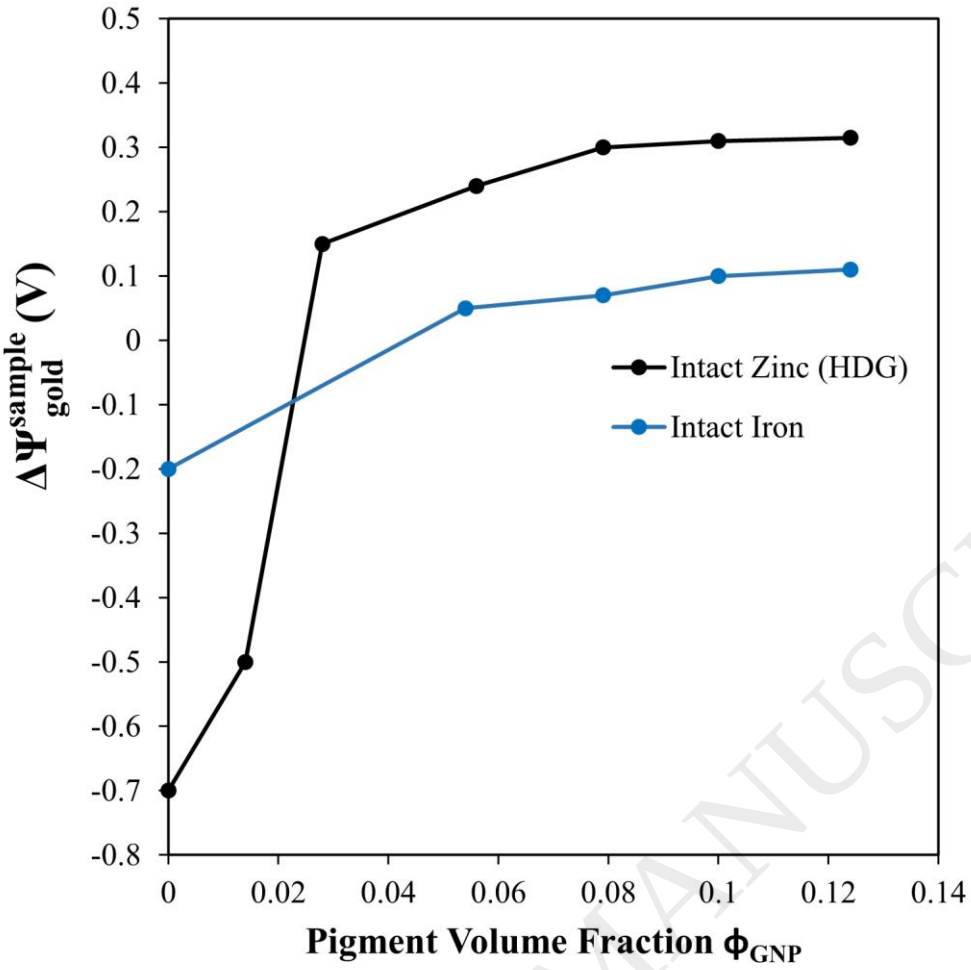

Fig. 4 A plot of the $\Delta\Psi^{sample}_{gold}$ profile vs. scan distance measured across a HDG substrate coated with a PVB layer and subsequently overcoated with the PVB-GNP composite at 0.056 ϕ_{GNP} with an overlaid schematic representative of the sample used in the experiment.

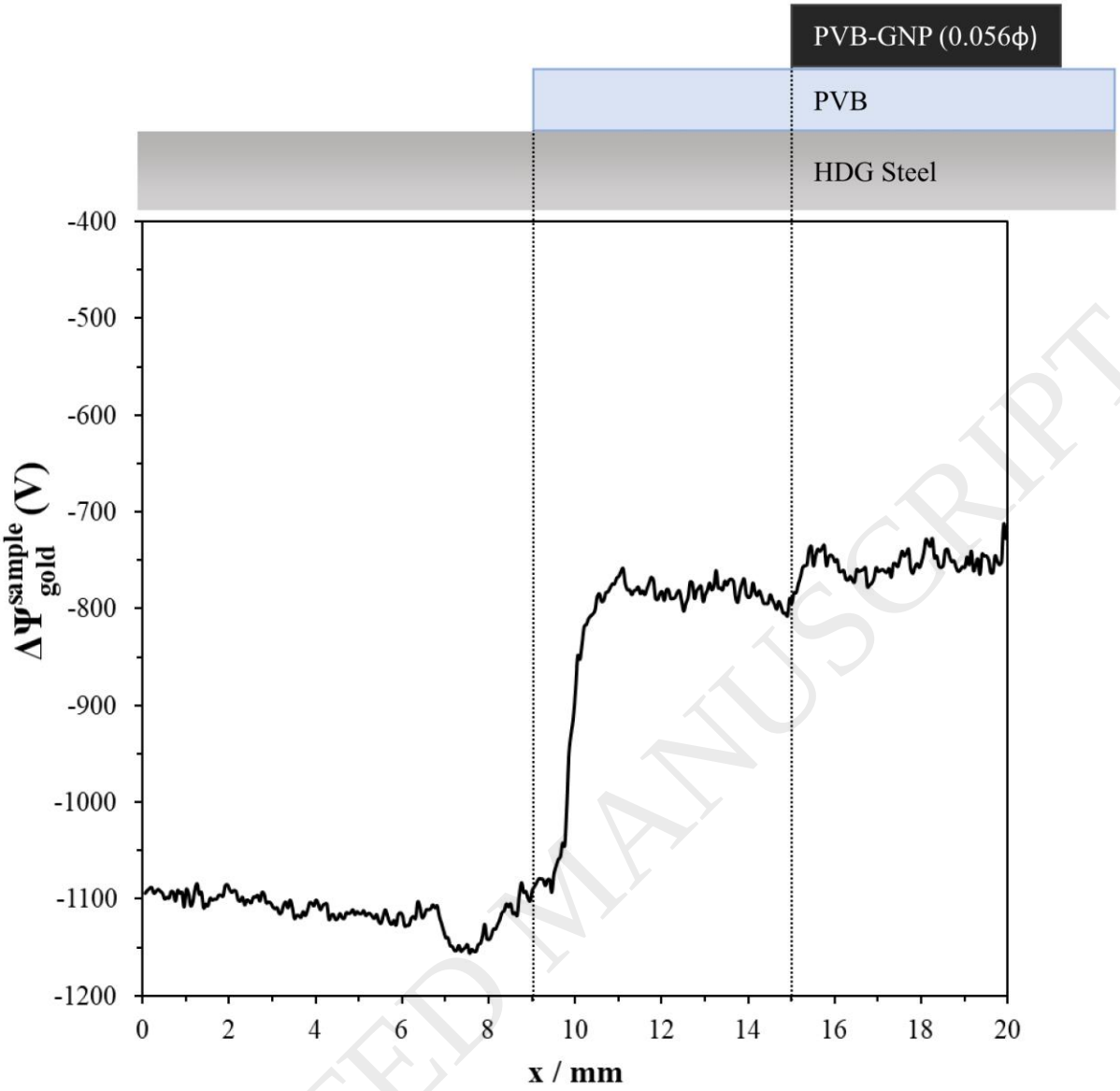

Fig. 5 Plots of time-dependent $\Delta\Psi^{sample}_{gold}$ vs. distance from the defect (*x*) profiles recorded for PVB coatings adherent to iron substrates where a) is the unpigmented coating given at 3 hourly intervals and b) containing 0.056 $\phi_{GNP,}$ shown at 4 hourly intervals, up to 24 h in both cases.

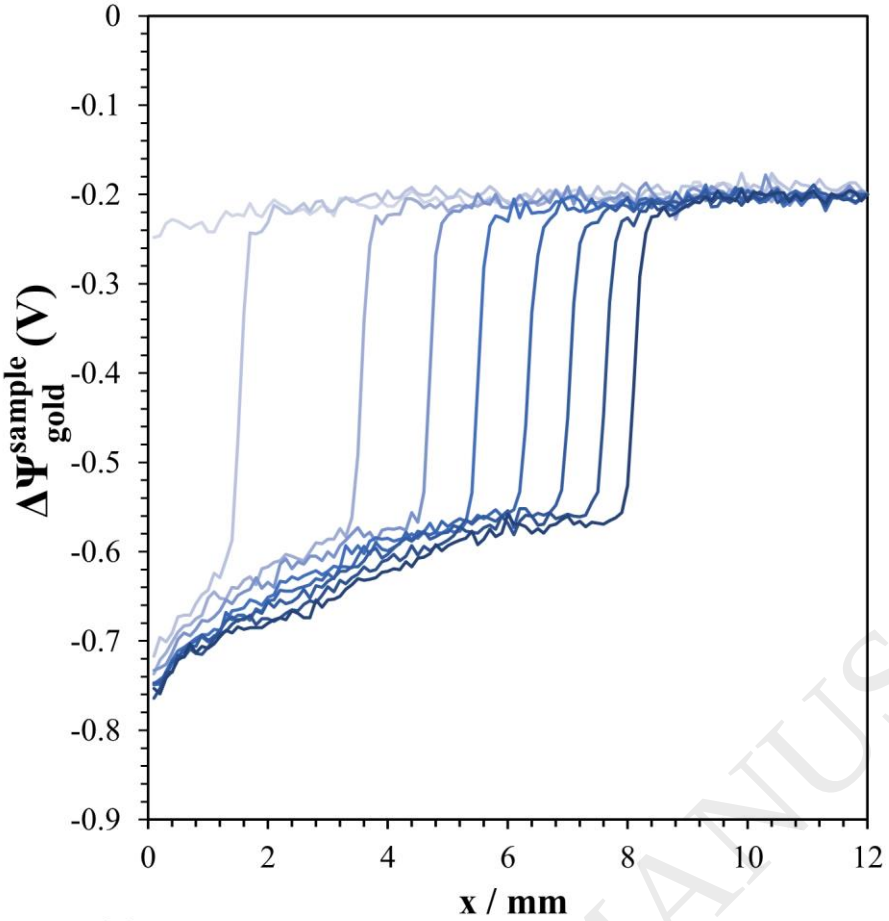

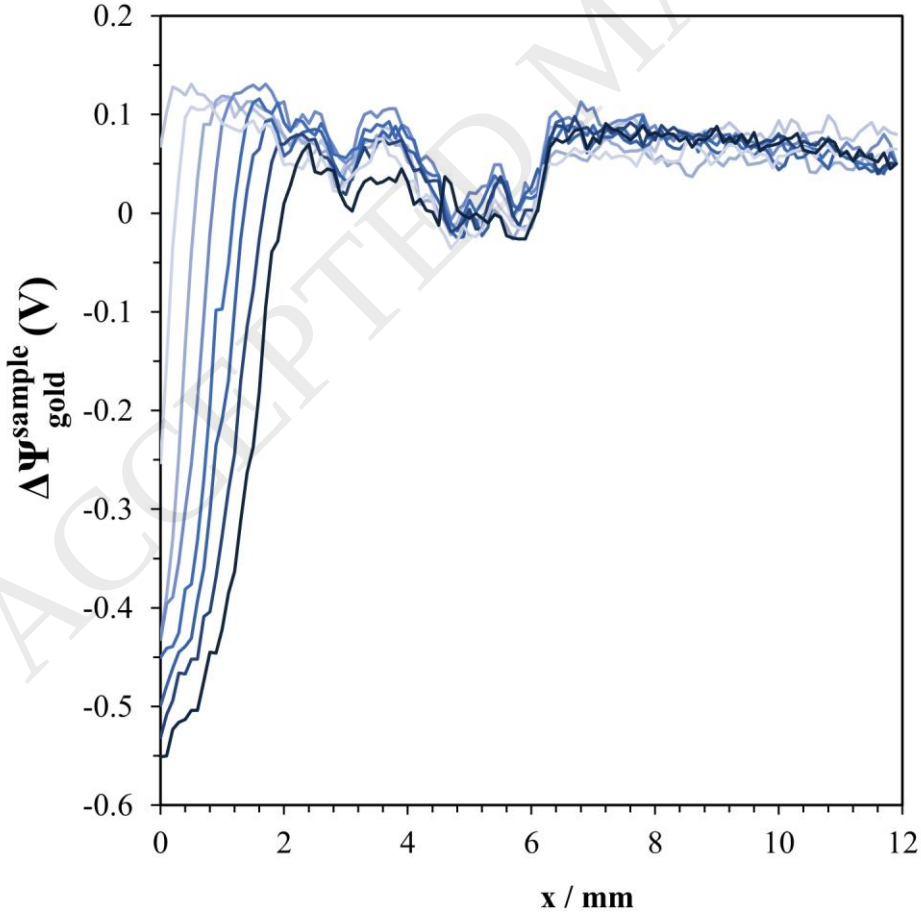

Fig. 6 Plots of delamination distance (x_{del}) as a function of time ($t - t_i$) for PVB coatings containing: i) 0 ϕ_{GNP}, ii) 0.028 ϕ_{GNP}, iii) 0.056 ϕ_{GNP}, iv) 0.079 ϕ_{GNP}, v) 0.1 ϕ_{GNP} and 0.124 ϕ_{GNP} on iron substrates where delamination was initiated by the introduction of 0.86 M aqueous NaCl electrolyte at pH 7.

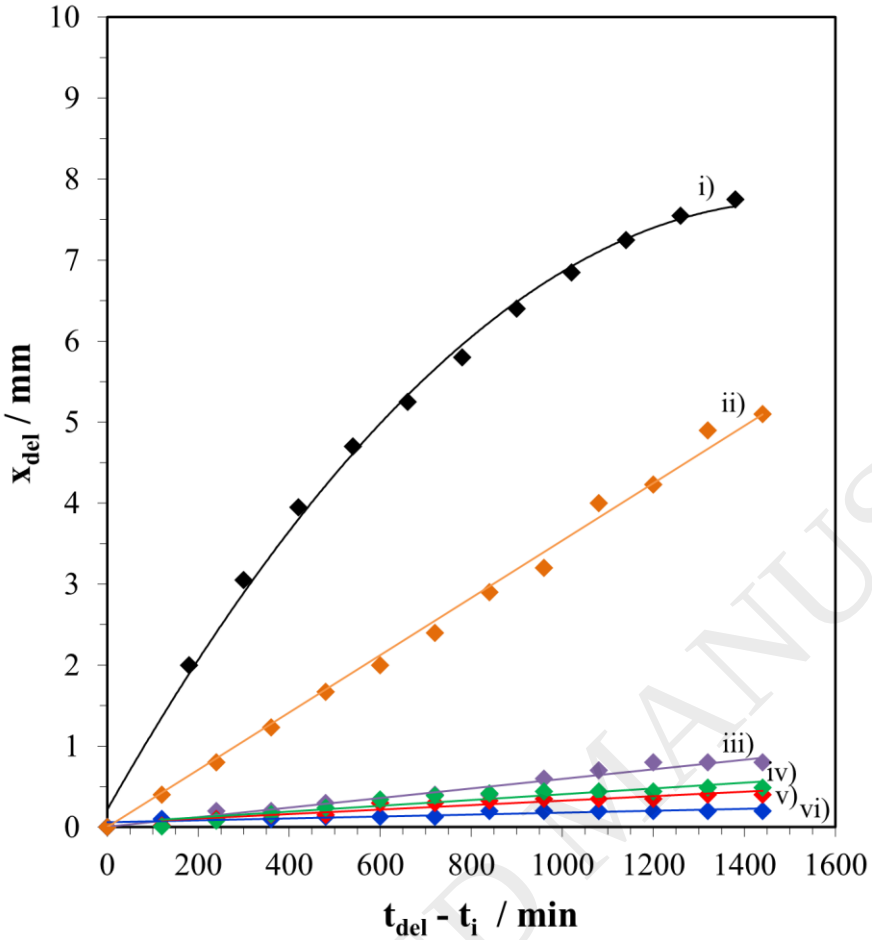

Fig. 7 Plots of time-dependent $\Delta\Psi_{gold}^{sample}$ vs. distance from the defect (x) profiles recorded for PVB coatings adherent to HDG substrates where a) is the unpigmented coating given at 3 hourly intervals and b) containing 0.028 $\phi_{GNP,}$ shown at 4 hourly intervals, up to 24 h in both cases.

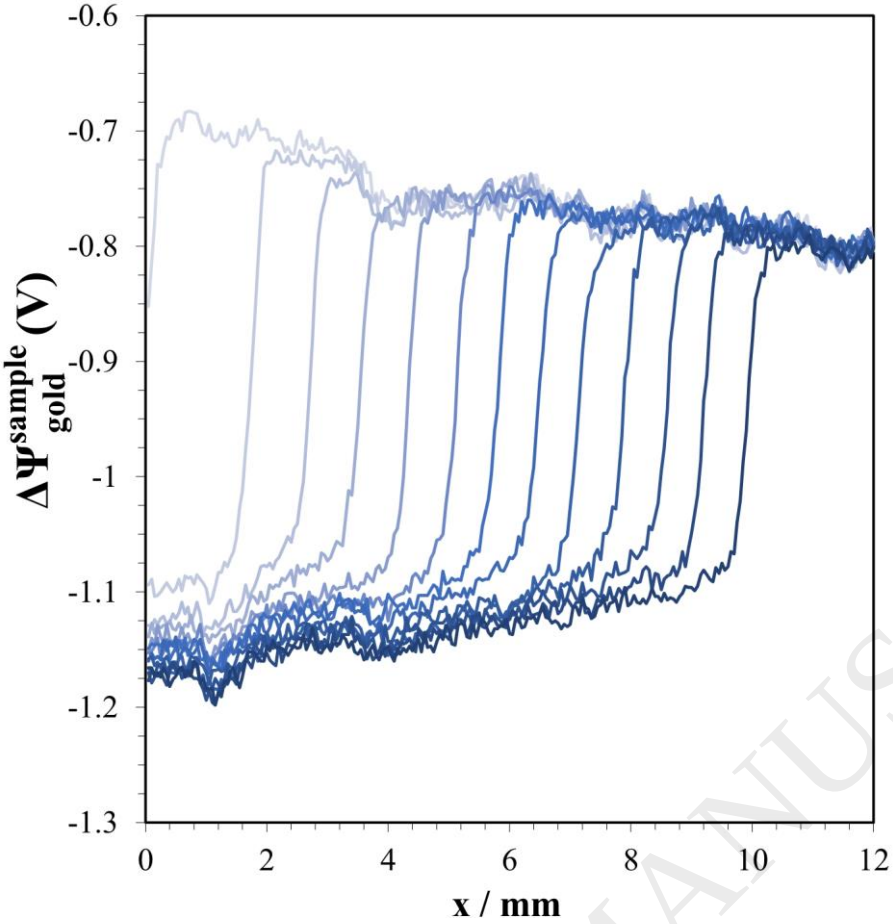

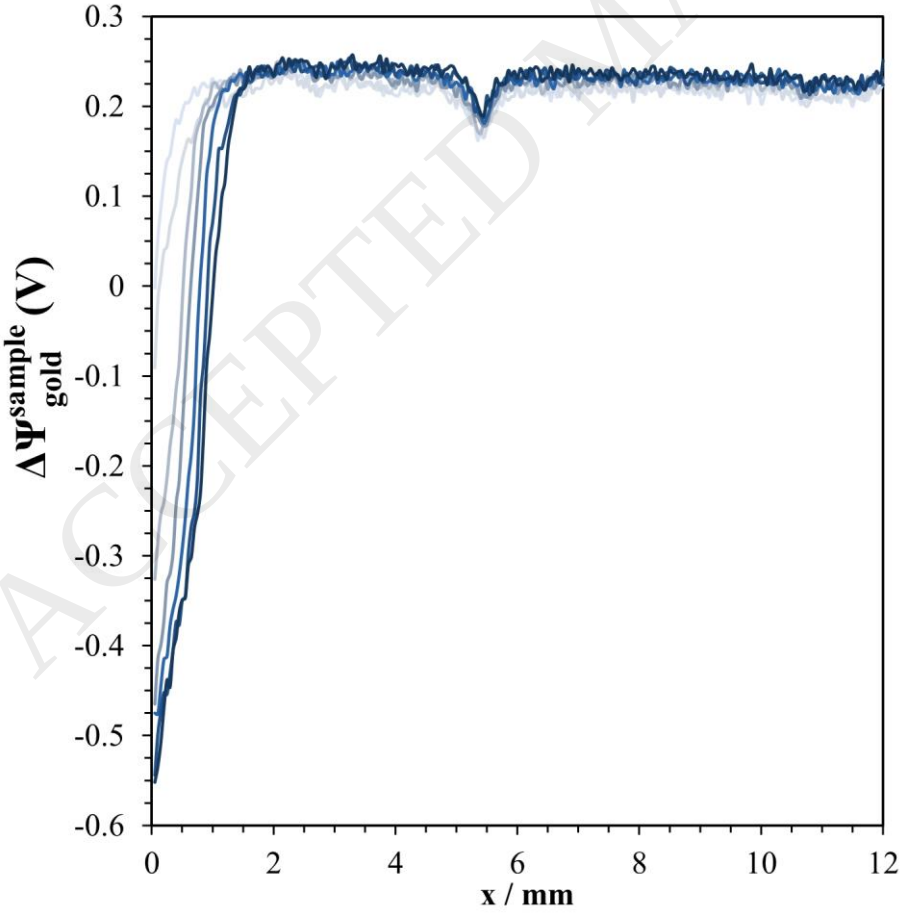

Fig. 8 Plots of delamination distance (x_{del}) as a function of time (t_{del} - t_i) for PVB coatings containing: i) 0 ϕ_{GNP}, ii) 0.007 ϕ_{GNP}, iii) 0.014 ϕ_{GNP}, iv) 0.028 ϕ_{GNP}, v) 0.056 ϕ_{GNP} on HDG substrates where delamination was initiated by the introduction of 0.86 M aqueous NaCl electrolyte at pH 7.

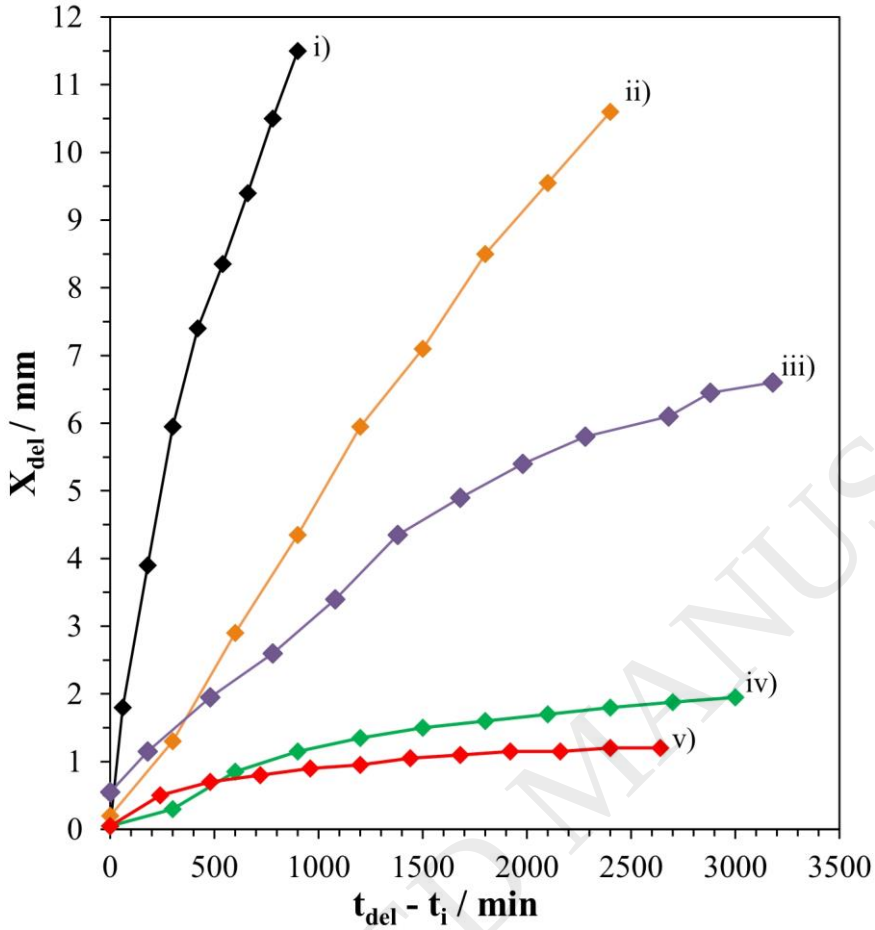

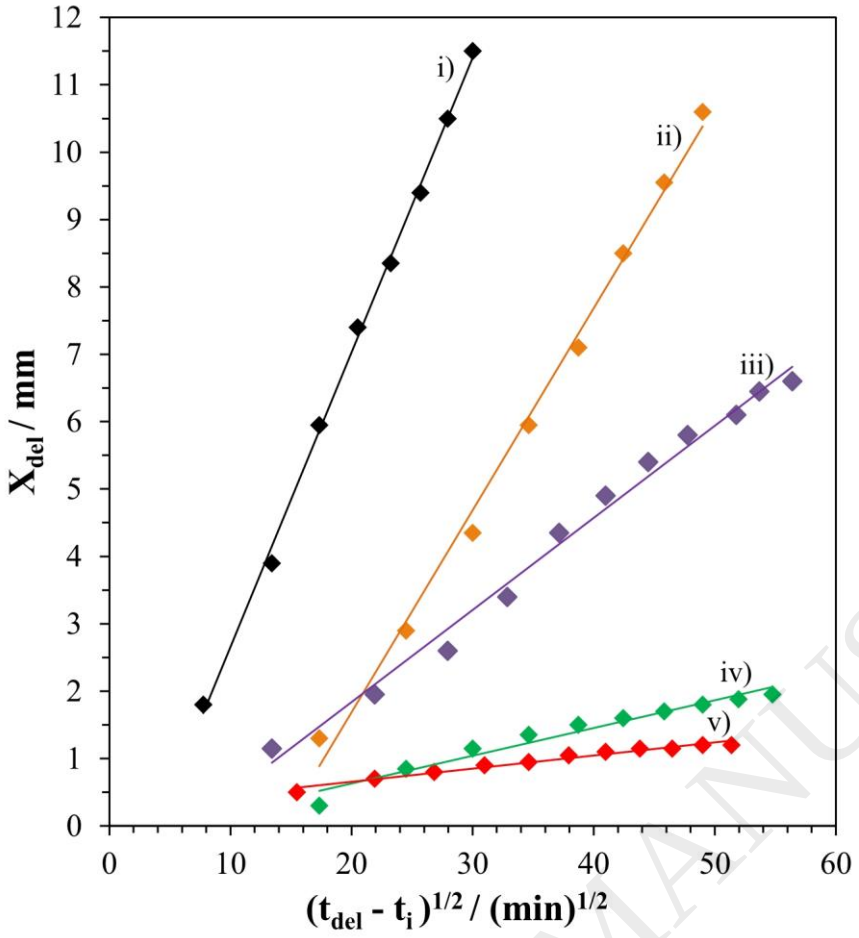

Fig. 9 Plots of the normalised values for (i) k_{del} of zinc (HDG), (ii) the delamination rates for iron and (iii) Oxygen Permeability as a function of ϕ_{GNP}.